HHS Public Access

Author manuscript

ASAIO J. Author manuscript; available in PMC 2020 July 01.

Published in final edited form as:

ASAIO J. 2019 July ; 65(5): 465–472. doi:10.1097/MAT.0000000000000835.

Wave Intensity Analysis of Right Ventricular Function during Pulsed Operation of Rotary Left Ventricular Assist Devices

J. Christopher Bouwmeester, PhD[*,#], **Jiheum Park, PhD**[†], **John Valdovinos, PhD**[§,#], and **Pramod Bonde, MD**[‡]

[*]Institute of Biomaterials and Biomedical Engineering, University of Toronto, Toronto, Canada

[†]Bonde Artificial Heart Laboratory, Department of Surgery, Yale School of Medicine, New Haven, CT

[§]Department of Electrical and Computer Engineering, California State University, Northridge, CA

[‡]Cardiac Surgery, Department of Surgery, Yale School of Medicine, New Haven, CT

[#]Formerly at Bonde Artificial Heart Laboratory, Department of Surgery, Yale School of Medicine, New Haven, CT

Abstract

Changing the speed of left ventricular assist devices (LVADs) cyclically may be useful to restore aortic pulsatility; however, the effects of this pulsation on right ventricular (RV) function are unknown. This study investigates the effects of direct ventricular interaction by quantifying the amount of wave energy created by RV contraction when axial and centrifugal LVADs are used to assist the left ventricle. In 4 anesthetized pigs, pressure and flow were measured in the main pulmonary artery and wave intensity analysis was used to identify and quantify the energy of waves created by the RV. The axial pump depressed the intensity of waves created by RV contraction compared to the centrifugal pump. In both pump designs, there were only minor and variable differences between the continuous and pulsed operation on RV function. The axial pump causes the RV to contract with less energy compared to a centrifugal design. Diminishing the ability of the RV to produce less energy translates to less pressure and flow produced which may lead to LVAD induced RV failure. The effects of pulsed LVAD operation on the RV appear to be minimal during acute observation of healthy hearts. Further study is necessary to uncover the effects of other modes of speed modulation with healthy and unhealthy hearts to determine if pulsed operation will benefit patients by reducing LVAD complications.

Keywords

Centrifugal blood pump; Axial blood pump; Pulsed operation; Wave intensity analysis; Right ventricular contraction

Corresponding author: Pramod Bonde, MD, FACS, Associate Professor of Surgery, Director of Mechanical Circulatory Support, Center for Advanced Heart Failure and Transplantation, Yale School of Medicine, Yale New Haven Hospital, 330 Cedar Street, 204 Boardman, PO Box: 208039, New Haven, CT 06520, Phone: (203) 785-6122, Fax: (203) 785-3346, pramod.bonde@yale.edu.

Conflicts of Interest: No relationships with industry to report.

Introduction

Right heart failure affects roughly a quarter of patients after LVAD implantation and in ~10 to 30% of patients there is a need for additional mechanical support.[1–5] The incidence of right ventricular (RV) failure remains difficult to predict because there are many factors that lead to RV failure.[6–8] In spite of careful patient selection, the incidence of RV failure following LVAD therapy has remained largely unchanged. Furthermore, RV function is an early indicator of long term mortality and therefore identifying RV dysfunction early is an important aspect of patient care. For these reasons RV failure remains an important factor that profoundly determines LVAD outcomes.

There is a clear need to provide more robust and quantitative metrics of RV dysfunction that provide objective criterion to diagnose the onset of RV failure. The current assessment of RV dysfunction is based solely on pressure and echocardiographic assessments, which are both operator dependent and variable. Thus, RV assessment remains primitive and difficult to assess dynamically over the course of patient care.

We are seeking to answer whether the wave energy provided by the heart can be quantified in the main pulmonary artery with the accuracy and precision necessary to determine the functional status of the heart and support a diagnosis of heart failure. The hypothesis driving this proposal is that right heart failure will result in the reduced wave energy produced by the RV compared to normal. This hypothesis is based on previous studies investigating the RV-pulmonary artery coupling and wave energy produced by the RV.[9, 10] Increased volume load and the concomitant increased cardiac output, via the Starling mechanism, resulted in approximately twice the amount of wave energy provided by the RV.[11] In similar volume loading conditions, other studies have quantified the contribution that wave reflections have to reduce peak systolic pressure, effectively facilitating RV ejection.[12, 13] Overall, studies that quantify the wave energy with wave intensity analysis (WIA) indicate that the RV produces more wave energy when cardiac output increases. Therefore, we believe that the resulting reduction of cardiac output caused by right heart failure will result in less energetic waves produced by the RV. Based on these assertions, the experimental focus of this proposal is to quantify the wave energy in the main pulmonary artery that is produced by a dysfunctional RV. The specific aims are designed to provide a comprehensive assessment of wave energy generated by the RV during baseline, increased preload, and increased afterload conditions.

Methods

Animal Preparation

The Yale University Institutional Animal Care and Use Committee granted approval of all experimental protocols. Four Yorkshire pigs (44 – 60 kg; mean 51 kg) were prepared based on a refined protocol that successfully provided anesthetic effects during entire period of experiments without loss of heart function, for example resulting in ventricular fibrillation[14].

Surgery and Instrumentation

A median sternotomy was used for the surgical approach, which was performed without the use of cardiopulmonary bypass. The pericardium was opened and was not reapproximated after LVAD implantation. Antiarrhythmic drugs (lidocaine 7 mg/kg and amiodarone 450 mg total) were administered in preparation for insertion of the inflow cannula into the left ventricle of the heart. A 34F (40 cm long) single-stage venous drainage cannula (Thin-Flex™; Edwards Lifesciences, Irvine, CA) was attached to the LVAD inflow and a 24 F (30 cm long) elongated one-piece arterial cannula (EOPA™; Medtronic, Minneapolis, MN) was attached to the LVAD outflow. Teflon pledgeted sutures were placed radially around the left ventricular apex and the inflow cannula tip was inserted and seated at the apex. The descending aorta was exposed and the outflow cannula was inserted using a modified Seldinger technique. In two animals a centrifugal LVAD was used (HVAD; HeartWare, Framingham, MA) and the other two animals an axial LVAD was used (HMII; Thoratec, Pleasanton, CA).

Pressure was measured in the ascending aorta, pulmonary artery, left atrium, and left and right ventricles. The 5F aortic catheter (Transonic Scisense Inc., London, Ontario, Canada) was inserted through the carotid artery and advanced to the ascending aorta. The high-fidelity catheter-tip transducer was referenced via its fluid-filled lumen to an external pressure transducer (ADIstruments, Colorado Springs, CO) connected to a four-channel bridge amplifier (ADInstruments). Zero pressure was defined as the midlevel plane of the heart with the animal in the supine position. A Swan-Ganz catheter (Edwards Lifesciences, Irvine, CA) was inserted in the jugular vein and advanced to the pulmonary artery to measure pressure in the main pulmonary artery. The distal port of the Swan-Ganz catheter was connected to an external pressure transducer. The left atrium as accessed by directly inserting a 3F catheter (Transonic Scisense Inc.) through the left atrial appendage. The left and right ventricles were accessed by directly inserting cannulas (20 Gauge Arterial Catheterization Set, Arrow International Inc., Reading, PA) through the anterior wall of the respective ventricle. Each ventricular cannula was attached to fluid-filled lines connected to external pressure transducers.

Flow was measured in the ascending aorta, pulmonary artery, and the LVAD outflow cannula. The 18 mm flow probes were placed (Confidence-series probes and flowmeter model TS420; Transonic Systems Inc., Ithaca, NY) on the main pulmonary artery (immediately downstream of the tip of the pulmonary artery catheter) and on the aorta (immediately upstream of the tip of the aortic catheter). An external clamp-on type flow sensor (8PXL-series; Transonic Systems Inc.) was used to measure flow in the LVAD outflow cannula. A 3-limb lead ECG was also recorded using an animal biological amplifier and needle electrodes (ADInstruments). Electronic signals were sampled at 400 Hz with data acquisition PowerLab hardware and LabChart software (ADInstruments) and filtered at 50 Hz using zero-phase digital filtering in Matlab (Mathworks Inc., Natick, MA).

Experimental Protocol

The goal of this study was to compare the effects of an LVAD on RV function during normal constant speed operation and speed modulated pulsation. Normal operation is defined by

setting the LVAD at a constant RPM. Pulsatile operation was defined by modulating the pump speed at a particular rate using a motor controller (Model TB6588FG; Toshiba) and custom designed user interface. Constant and pulsatile operation is represented in Figure 1, which shows that the natural cardiac cycle was approximated by specifying systole to be 30% and diastole to be 70% of the pump cycle. For the centrifugal LVAD the following pump speeds were used: constant speed = 2700 rpm; systolic speed = 3400 rpm; diastolic speed = 2300 rpm. For the axial LVAD the following pump speeds were used: constant speed = 7000 rpm; systolic speed = 6600 rpm; diastolic speed = 7800 rpm.

Data were acquired during stable hemodynamic conditions and the LVAD was operated at a constant speed mode (i.e. control) for 30 seconds and then switched to pulsatile mode. The constant RPM set during control conditions was designed to be approximately equal to the mean RPM during pulsatile operation. The rate of pulsatile pumping was set to be 10% slower than the intrinsic heart rate (as measured during the first 30 seconds of data acquisition). Setting the LVAD to pump asynchronously at 10% of the intrinsic heart rate allowed for the LVAD to pump in phase with the heart (i.e. co-pulsation) and out of phase with the heart (i.e. counter-pulsation).

During each intervention (i.e., baseline, increased afterload, and increased preload), pulsatile operation of the LVAD was compared to a control state where the pump was operated normally at a constant RPM. Baseline conditions were measured after the animal reached hemodynamic stability after surgery. Norepinephrine (0.33 – 1.0 μg/kg·min) was used subsequently to increase afterload and after a period of weaning the animal off norepinephrine and a return to baseline conditions, a bolus of approximately 500 mL of Vetastarch (6% hydroxyethyl starch) via a jugular cannula was used to increase preload by raising LV end-diastolic pressure from approximately 5 mmHg (during baseline) to approximately 10 mmHg. This level of volume loading was maintained with further infusions of normal saline.

Data Analysis

In this study, wave intensity analysis[15,16] was used to calculate the energy associated with waves measured in the main pulmonary artery. In terms of wave intensity analysis, waves create incremental changes in pressure and flow and net wave intensity (dI) and wave energy (I) are calculated as follows:

$$dI = dP dU \quad \text{Equation 1}$$

$$I = \int_{t_{start}}^{t_{end}} dI\, dt \quad \text{Equation 2}$$

Net wave intensity has units of W/m^2 and net wave energy is used to quantify wave energy during a period of interest (i.e. from t_{start} to t_{end}) and has units of J/m^2. dP and dU are the

incremental changes in pressure and velocity respectively. Velocity was determined by dividing flow by the cross-sectional area of the blood vessel; the diameter of which was estimated by the size of flow probe used to measure flow.

Single-point wave speed (c) was calculated using the linear regression method,[17] where it is assumed that only one wave is present during the upstroke of systole and the density of blood (ρ) is 1040 kg/m^3. The linear relationship of pressure and velocity during this period is used to determine the wave speed and decompose wave intensity, pressure, and velocity into forward-going (+) and backward-going (−) wave components.[18]

$$dI_{\pm} = \pm \frac{1}{4\rho c}(dP \pm \rho c dU)^2 \quad \text{Equation 3}$$

$$dP_{\pm} = \pm \frac{1}{2}(dP \pm \rho c dU) \quad \text{Equation 4}$$

$$dU_{\pm} = \pm \frac{1}{2}\left(dU \pm \frac{dP}{\rho c}\right) \quad \text{Equation 5}$$

Wave intensity analysis defines 4 characteristic waves which can be identified by incremental changes in pressure and velocity/flow. A forward compression wave (FCW) increases pressure and velocity and a forward decompression wave (FDW) decreases pressure and velocity. A backward compression wave (BCW) increases pressure and decreases flow and a backward decompression wave (BDW) decreased pressure and increases flow.

Applying WIA to measurements made in the main pulmonary artery is shown in Figure 2. Panel A shows pressure and flow waveforms. Panel B displays the resulting net wave intensity, in this case positive wave intensity indicates that forward-going waves dominate throughout the cycle. Panel C displays the decomposition of net wave intensity into forward- and backward-going components and shows that backward waves are indeed minimal. The two major waves created by the RV are labeled; the FCW is caused by RV contraction and is followed by a FDW which is caused by the start of RV relaxation.[16, 19] These waves can be quantified by the peak net wave intensity of the FCW and FDW and the integrated area beneath each wave.

Statistical Methods

Three pump modes (control, counter-pulsation, and co-pulsation) were compared using one-way ANOVA. Representative samples from the data were collected by using 30 consecutive cardiac cycles selected from constant speed operation and 30 cardiac cycles selected when the LVAD was in phase (i.e. co-pulsation) and out of phase (i.e. counter-pulsation) with the heart. For all statistical tests the significance level was set at 0.05 and if the results from one-

way ANOVA were significant (i.e. $p < 0.05$), then multiple comparisons between each group were made with the Bonferroni post-hoc test.

Results

The effects of constant and speed modulated pulsation on LVAD flow are shown in Figure 3. Counter-pulsation leads to a decrease in pump flow amplitude and co-pulsation causes an increase in pump flow amplitude. Tables 1 and 2 summarize basic hemodynamic data when the LVAD was in continuous and pulsed mode during each intervention (i.e., baseline, increased preload, and increased afterload). Average values for systolic, diastolic aortic pressures, and the average heart rate are shown in Table 1, and the cardiac output (i.e., average aortic flow) and LVAD flow (i.e., average pump flow) are shown in Table 2.

The effects that a centrifugal and axial LVAD have on the wave intensity produced by the RV are shown in Figure 4A. The main difference between the wave patterns is that the FCW generated by the RV is depressed when the axial LVAD was implanted. The effects of each pump mode (i.e. constant, co-pulsation, and counter-pulsation) are shown in Figure 4B. For both pump designs, both co- and counter-pulsation had negligible effects on the wave patterns. The effects of increasing afterload with norepinephrine and increasing preload with volume loading are shown in Figure 4C. Peak wave intensity of both the FCW and FDW appear to rise when afterload is increased, with greater rises observed when the centrifugal LVAD was implanted. In each of these figures, each representative waveform is a single beat that was chosen because it had the smallest mean-squared error compared to an ensemble averaged beat during each pumping mode and hemodynamic condition. To account for differences in heart rate and compare each hemodynamic condition, the time axis is normalized to represent a single cardiac cycle.

Table 3 summarizes metrics that can be used to define the waves created by the RV. Data are listed for each experiment and the differences between control, co-pulsation, and counter-pulsation are compared during each intervention. The strength of waves created by RV contraction are defined by the maximum value of the FCW and the strength of waves created by start of RV relaxation are defined by the maximum value of the FDW, as shown in Table 3. Low intensity waves of longer duration can have equal importance as high intensity waves of short duration and therefore, the forward wave energy (i.e. integrated area of the FCW plus FDW) is shown in Table 3. Net wave intensity was separated into forward and backward components (see Figure 2). Backward wave intensity is negligible during the identified FCW and FDW and therefore, the values of net wave intensity reported in Table 3 were representative of the waves generated by the RV. The single point wave speed was calculated and negligible differences were observed between control and pulsatile pump modes.

Discussion

The goal of this study was to investigate the potential of WIA to measure the effects that LVADs have on the wave patterns produced by the right ventricle. The effects of a centrifugal and axial LVAD were analyzed during normal operation (i.e. a constant pump

speed) and during asynchronous pulsatile operation (i.e. co- and counter-pulsation). These pumping modes were tested during different physiological interventions that increased preload (with volume loading) and afterload (with norepinephrine).

The major finding of this study is that centrifugal and axial pumps may have different effects on the RV and have the potential to create different wave patterns. The axial pump appears to depress the waves created by RV contraction (i.e. the FCW) compared to the centrifugal pump. Furthermore, the response to increased afterload when the axial pump was implanted was not as great compared to the centrifugal pump. These results indicate that different pump designs have the potential to alter the strength of waves created by RV contraction and further work is warranted to define the effects that LVADs have on RV function over a range of physiologic interventions.

Differences between Pumps

The normal wave intensity pattern in the main pulmonary artery is characterized by a relatively large magnitude FCW followed by a comparatively smaller FDW,[9, 10, 12, 20, 21] somewhat similar to the wave intensity shown in Figure 2. As shown in Figure 4A, the centrifugal pump appears to preserve the characteristic wave pattern that the RV would be expected to produce. Alternatively, the axial pump appears to depress the FCW substantially but preserve the strength of the FDW. The FCW is a marker for the strength of RV contraction and the ability to accelerate blood flow in the pulmonary artery. Therefore, the ability of the axial pump compared to the centrifugal pump to depress peak FCW intensity suggests that the RV does not contract as forcefully when an axial pump is implanted in the LV. Previous work has shown that peak wave intensity is positively related to changes in contractility[19] and the assertion that a reduction in peak FCW intensity indicated reduced RV contractility is supported by studies that have shown impaired RV contractility when the LV was bypassed.[22–24] Therefore, it is possible that the reduction in peak FCW intensity with the axial pump indicates a reduction in RV contractility. This observation is also supported by the nature of axial LVAD designs to potentially generate greater inlet suction compared to centrifugal LVAD designs. The steeper HQ curve of a typical axial LVAD would allow greater pressure to be developed at low flow conditions and the flatter HQ curve of a typical centrifugal LVAD would likely reduce potential suction events.[25–27]

Differences between Control and Pulsatile Pumping

Few studies have investigated the effects that pulsatile pumping of continuous flow LVADs have on the RV. A modelling study provides some evidence that counter-pulsation results in a beneficial reduction in RV work by reducing afterload[28] and animal studies have shown that counter-pulsation results in the greatest degree of leftward septal shift while maintaining maximum flow support.[29, 30] Therefore, the timing of LVAD pulsation and degree of leftward septal shift are key to hypothesizing what effects co- or counter-pulsation may have on the RV and the forward wave intensity it can generate. We would hypothesize that counter-pulsation could cause increased forward wave intensity compared to control conditions. If RV end-diastolic volume increases from leftward septal shifts during diastole (as counter-pulsation pumps relatively more blood from the LV during diastole), then the Frank-Starling mechanism will cause greater RV contractility and increased forward wave

intensity. We would hypothesize that co-pulsation could cause decreased forward wave intensity compared to control conditions. If a leftward septal shift occurs during systole (as co-pulsation pumps relatively more blood from the LV during systole), then impaired septal contraction will cause decreased RV contractility and decreased forward wave intensity.

As shown in Figure 4B, there are negligible differences between control, co-, and counter-pulsation wave intensity patterns and therefore there appear to be no observable changes in RV function. The likely reason that no changes could be detected is that this study investigated acute changes in healthy animals, while previous studies use a model of bi-ventricular dysfunction created by injection microspheres into the left anterior descending and right coronary arteries.[29] Furthermore, the pericardium was removed during in this study during experimentation and this would have decreased the effects that septal shifts have on mediating the hypothesized effects of direct ventricular interaction.

Differences between Physiological Interventions

Increasing the amount of preload with an acute infusion of volume had negligible effects on the intensity or energy of waves created by the RV. Normally, it would be expected that additional preload would cause an increase of contractility via the Frank-Starling mechanism and result in greater wave intensity created by the RV. This behavior is observed for the LV but the results of this study suggest that the RV is not as sensitive as the LV to an increase in preload.

Similar to the effects of dobutamine, [19, 31] an increase in afterload with norepinephrine in this study caused an increase in wave intensity of the FCW and FDW produced by the RV. This suggests that the inotropic effect of norepinephrine (i.e., increased ventricular contractility) increases the intensity of forward waves and outweighs any vasopressor effects that would otherwise serve to depress the intensity of forward waves.[19] The increase of afterload also increases the pump head pressure and appears to have an effect on lowering LVAD flow (as Table 2 seems to suggest). We hypothesize that this may enable the septum to contribute more to RV contraction and greater intensity of FCWs.

Limitations

Further wave analysis using the excess pressure defined by the reservoir-wave model[32, 33] was not performed as the increases in heart rate and the perturbations caused by pulsatile pumping did not allow the reservoir pressure to be calculated consistently.

The wave patterns created by the RV were not measured prior to LVAD implantation. Therefore, the changes in the characteristic RV wave pattern before and after LVAD surgery were not measured. Heart function with the LVAD turned off (and the inflow/outflow cannulas clamped) could have been measured but concerns related to the stasis of blood in the pump and the formation of blood clots dictated the decision to not test this option. While the comparisons between the ability of centrifugal and axial pumps to influence RV generated wave patterns is still valid, further studies could be designed to quantify the characteristic wave patterns before and after LVAD implantation.

This study focused on the differences between centrifugal and axial LVADs and control versus pulsatile pumping in each design. This study did not compare different continuous pump speeds or different ranges of speed modulation. It could be hypothesized that higher pump pulsatility would have greater effects on the RV. Future studies could be designed to investigate other ranges of speed modulated pulsatility.

Periods of co- and counter-pulsation were identified post-hoc by the pattern created by LVAD outflow (see Figure 3). The asynchronous pulsatility used in this study may be different from synchronous pulsatility. Unlike previous studies that used the ECG to sync pulsatile pump flow with the intrinsic heart rate,[34] in this study asynchronous pulsatility was used primarily because of technical difficulties related to the pump controller deficiencies in measuring the ECG signal in real time and adjusting to the natural changes in intrinsic heart rate. While synchronous pulsatility in either co- or counter-pulsation mode has the potential to have greater repeatability, this study used at least 5 minutes of data collection during asynchronous pulsatility to obtain enough individual cardiac cycles related to co- and counter-pulsation.

Conclusions

Centrifugal and axial pumps interact with the RV in different and important ways. The major difference is that the axial pump design appears to cause a relatively depressed FCW. The depressed FCW indicates that the strength of RV contraction is reduced when the axial pump is implanted in the LV and suggests that the greater suction of an axial LVAD serves to reduce impaired RV contractile function. The characterization of RV wave patterns over a range of physiologic conditions for both centrifugal and axial pumps is important to provide new methods to measure the effects that LVADs have on RV function.

Acknowledgments

Source of Funding: The project described was supported by NIH/NHLBI grant# R21HL118611

References

1. Kirklin JK, Naftel DC, Pagani FD, Kormos RL, Stevenson LW, et al. Sixth intermacs annual report: A 10,000-patient database. Journal of Heart and Lung Transplantation. 2014; 33:555–564. [PubMed: 24856259]
2. Dang NC, Topkara VK, Mercando M, Kay J, Kruger KH, et al. Right heart failure after left ventricular assist device implantation in patients with chronic congestive heart failure. Journal of Heart and Lung Transplantation. 2006; 25:1–6. [PubMed: 16399523]
3. Potapov EV, Stepanenko A, Dandel M, Kukucka M, Lehmkuhl HB, et al. Tricuspid incompetence and geometry of the right ventricle as predictors of right ventricular function after implantation of a left ventricular assist device. Journal of Heart and Lung Transplantation. 2008; 27:1275–1281. [PubMed: 19059106]
4. Morgan JA, John R, Lee BJ, Oz MC, Naka Y. Is severe right ventricular failure in left ventricular assist device recipients a risk factor for unsuccessful bridging to transplant and post-transplant mortality. Annals of Thoracic Surgery. 2004; 77:859–863. [PubMed: 14992887]
5. Furukawa K, Motomura T, Nose Y. Right ventricular failure after left ventricular assist device implantation: The need for an implantable right ventricular assist device. Artificial Organs. 2005; 29:369–377. [PubMed: 15854212]

6. Bonde P, Ku NC, Genovese EA, Bermudez CA, Bhama JK, et al. Model for end-stage liver disease score predicts adverse events related to ventricular assist device therapy. Annals of Thoracic Surgery. 2012; 93:1541–1547. [PubMed: 22480391]
7. Wang Y, Simon M, Bonde P, Harris BU, Teuteberg JJ, et al. Prognosis of right ventricular failure in patients with left ventricular assist device based on decision tree with smote. IEEE Transactions on Information Technology in Biomedicine. 2012; 16:383–390. [PubMed: 22334033]
8. Wang Y, Simon MA, Bonde P, Harris BU, Teuteberg JJ, et al. Decision tree for adjuvant right ventricular support in patients receiving a left ventricular assist device. Journal of Heart and Lung Transplantation. 2012; 31:140–149. [PubMed: 22168963]
9. Hollander EH, Wang JJ, Dobson GM, Parker KH, Tyberg JV. Negative wave reflections in pulmonary arteries. American Journal of Physiology: Heart and Circulatory Physiology. 2001; 281:H895–H902. [PubMed: 11454596]
10. Smolich JJ, Mynard JP, Penny DJ. Simultaneous pulmonary trunk and pulmonary arterial wave intensity analysis in fetal lambs: Evidence for cyclical, midsystolic pulmonary vasoconstriction. American Journal of Physiology: Regulatory, Integrative and Comparative Physiology. 2008; 294:R1554–R1562.
11. Dwyer, N. Doctor of Philosophy. 2010. Pulmonary arterial wave intensity analysis in health and disease. Faculty of health science; 193
12. Bouwmeester JC, Belenkie I, Shrive NG, Tyberg JV. Wave reflections in the pulmonary arteries analysed with the reservoir-wave model. Journal of Physiology. 2014
13. Bouwmeester, JC. Biomedical Engineering. 2012. Reservoir-wave analysis applied to the pulmonary circulation; 185Ph.D
14. Goodrich JA, Bouwmeester C, Letzen B, Waters B, Smith J, Bonde P. Refinement of an anesthesia protocol fora porcine model for a FREE-D powered ventricular assist device. J Invest Surg. 28:60.2015;
15. Parker KH, Jones CJH. Forward and backward running waves in the arteries: Analysis using the method of characteristics. Journal of Biomechanical Engineering. 1990; 112:322–326. [PubMed: 2214715]
16. Parker KH, Jones CJH, Dawson JR, Gibson DG. What stops the flow of blood from the heart? Heart and Vessels. 1988; 4:241–245. [PubMed: 3254905]
17. Khir AW, O'Brien A, Gibbs JSB, Parker KH. Determination of wave speed and wave separation in the arteries. Journal of Biomechanics. 2001; 34:1145–1155. [PubMed: 11506785]
18. Parker KH. An introduction to wave intensity analysis. Medical and Biological Engineering and Computing. 2009; 47:175–188. [PubMed: 19205773]
19. Jones CJ, Sugawara M, Kondoh Y, Uchida K, Parker KH. Compression and expansion wavefront travel in canine ascending aortic flow: Wave intensity analysis. Heart and Vessels. 2002; 16:91–98. [PubMed: 12027238]
20. Dwyer N, Yong AC, Kilpatrick D. Variable open-end wave reflection in the pulmonary arteries of anesthetized sheep. Journal of Physiological Sciences. 2012; 62:21–28. [PubMed: 22102164]
21. Nie M, Kobayashi H, Sugawara M, Tomita T, Ohara K, et al. Helium inhalation enhances vasodilator effect of inhaled nitric oxide on pulmonary vessels in hypoxic dogs. American Journal of Physiology: Heart and Circulatory Physiology. 2001; 280:H1875–1881. [PubMed: 11247804]
22. Moon MR, Castro LJ, DeAnda A, Tomizawa Y, Daughters GT 2nd, et al. Right ventricular dynamics during left ventricular assistance in closed-chest dogs. Annals of Thoracic Surgery. 1993; 56:54–66. [PubMed: 8328877]
23. Fukamachi K, Asou T, Nakamura Y, Toshima Y, Oe M, et al. Effects of left heart bypass on right ventricular performance. Evaluation of the right ventricular end-systolic and end-diastolic pressure-volume relation in the in situ normal canine heart. Journal of Thoracic and Cardiovascular Surgery. 1990; 99:725–734. [PubMed: 2319796]
24. Santamore WP, Gray LA Jr. Left ventriuclar contributions to right ventricular systolic function during lvad support. Ann Thorac Surg. 1996; 61:350–356. [PubMed: 8561604]
25. Giridharan GA, Koenig SC, Soucy KG, Choi Y, Pirbodaghi T, et al. Left ventricular volume unloading with axial and centrifugal rotary blood pumps. ASAIO Journal. 2015; 61:292–300. [PubMed: 25635936]

26. Moazami N, Fukamachi K, Kobayashi M, Smedira NG, Hoercher KJ, et al. Axial and centrifugal continuous-flow rotary pumps: A translation from pump mechanics to clinical practice. Journal of Heart and Lung Transplantation. 2013; 32:1–11. [PubMed: 23260699]
27. Stanfield JR, Selzman CH. In vitro pulsatility analysis of axial-flow and centrifugal-flow left ventricular assist devices. Journal of biomechanical engineering. 2013; 135:034505.
28. Poullis M. Pulsatile mode of operation of left ventricular assist devices and pulmonary haemodynamics. Interactive Cardiovascular and Thoracic Surgery. 2014; 19:11–15. [PubMed: 24722514]
29. Arakawa M, Nishimura T, Takewa Y, Umeki A, Ando M, et al. Novel control system to prevent right ventricular failure induced by rotary blood pump. J Artif Organs. 2014; 17:135–141. [PubMed: 24504544]
30. Fukuda S, Takano H, Taenaka Y, Nakatani T, Noda H, et al. Chronic effect of left ventricular assist pumping on right ventricular function. ASAIO Transactions. 1988; 34:712–715. [PubMed: 3196588]
31. Penny DJ, Mynard JP, Smolich JJ. Aortic wave intensity analysis of ventricular-vascular interaction during incremental dobutamine infusion in adult sheep. American Journal of Physiology: Heart and Circulatory Physiology. 2008; 294:H481–489. [PubMed: 18024544]
32. Tyberg JV, Bouwmeester JC, Parker KH, Shrive NG, Wang JJ. The case for the reservoir-wave approach. International Journal of Cardiology. 2014
33. Wang JJ, O'Brien AB, Shrive NG, Parker KH, Tyberg JV. Time-domain representation of ventricular-arterial coupling as a windkessel and wave system. American Journal of Physiology: Heart and Circulatory Physiology. 2003; 284:H1358–H1368. [PubMed: 12531729]
34. Ando M, Nishimura T, Takewa Y, Yamazaki K, Kyo S, et al. Electrocardiogram-synchronized rotational speed change mode in rotary pumps could improve pulsatility. Artificial Organs. 2011; 35:941–947. [PubMed: 21615427]

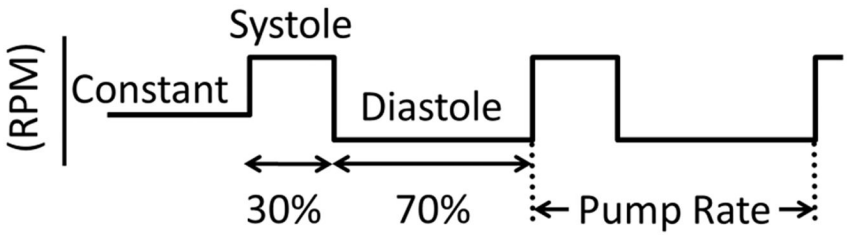

Figure 1. Schematic representation of LVAD pump speeds

When the centrifugal pump was used: constant speed = 2700 rpm, systolic speed = 3400 rpm, and diastolic speed = 2300 rpm. When the axial pump was used: constant speed = 7000 rpm, systolic speed = 7800 rpm, and diastolic speed = 6600 rpm.

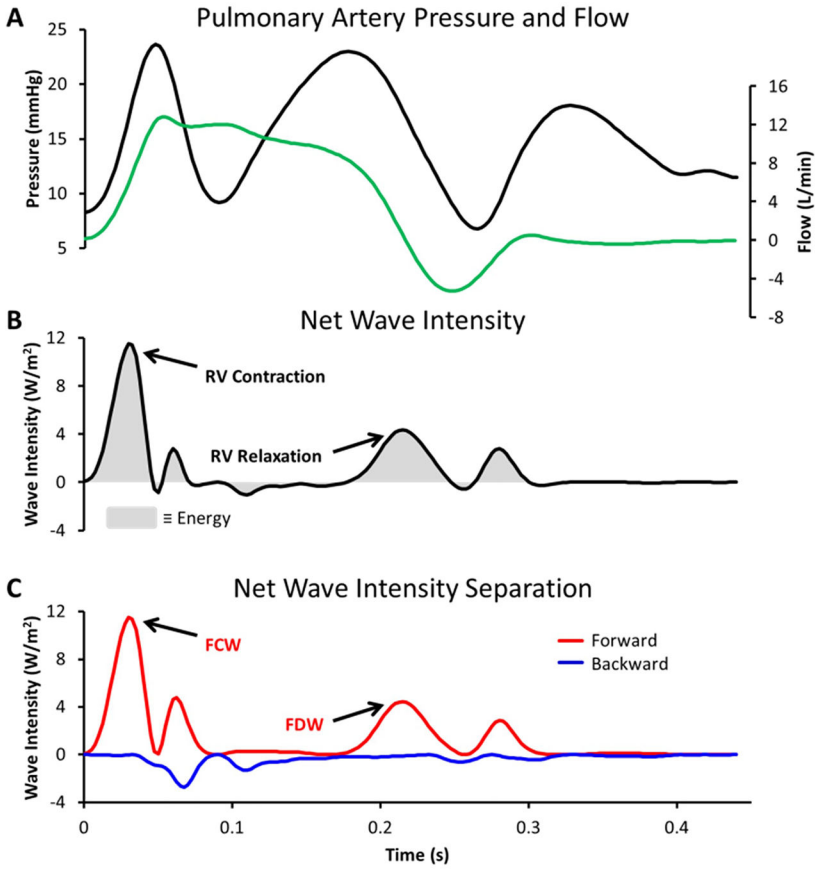

Figure 2. Example of wave intensity analysis when a centrifugal LVAD was implanted

Panel A: Main pulmonary artery pressure and flow waveforms are shown for one cardiac cycle. Panel B: Calculated net wave intensity is labeled with the 2 major waves created by the right ventricle. Wave energy is represented by the grey shaded area. Panel C: Net wave intensity is separated into the contributions of forward- (red line) and backward-going (blue line) waves. The forward compression wave (FCW) and decompression wave (FDW) created by the right ventricle are labeled.

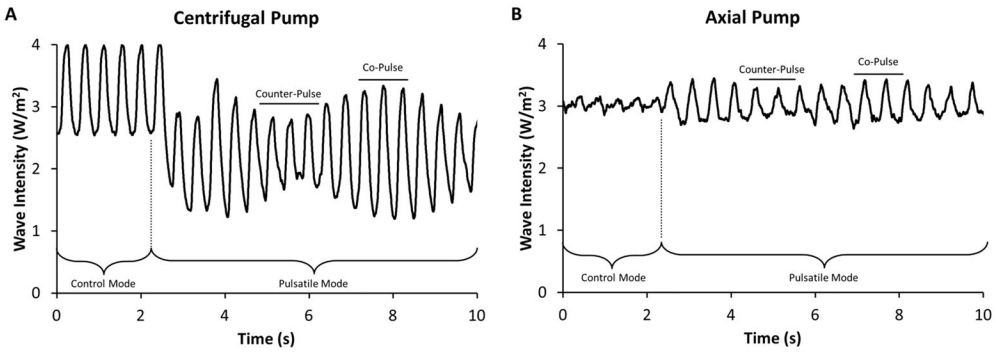

Figure 3. LVAD outflow patterns during control and asynchronous pulsatile operation

The different LVAD outflow patterns for the centrifugal pump (Panel A) and the axial pump (Panel B) are shown during the initial transition between control and pulsatile modes of operation. The difference between the intrinsic heart rate and pulsatile LVAD rate result in the amplitude changes of pump flow. Co-pulse is identified by the individual cardiac cycles with high amplitude and counter-pulse is identified by the individual cardiac cycles with low amplitude.

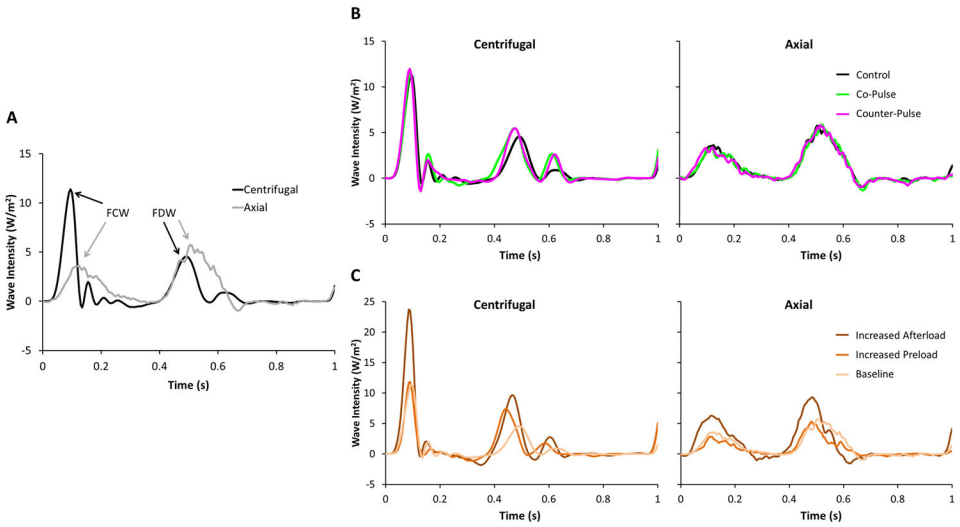

Figure 4. Main pulmonary artery wave intensity patterns with centrifugal and axial pumps

(A) The net wave intensity is shown during baseline physiologic conditions and control mode (i.e. constant pump speed). The peak intensity of the forward compression wave (FCW) and forward decompression wave (FDW) are labeled. The time domain is normalized to compare cardiac cycles (0 = start; 1 = end) with different heart rates. (B) Effects of pulsatile pump operation on wave intensity patterns are shown during baseline physiologic conditions. Control (i.e. constant speed), co-pulse, and counter-pulse (i.e. speed modulation) modes are indicated by the colored lines. The time domain is normalized to compare cardiac cycles (0 = start; 1 = end) with different heart rates. (C) Effects of physiological interventions on wave intensity patterns are shown during control mode (i.e. constant speed). Each physiologic condition is indicated by the colored lines. The time domain is normalized to compare cardiac cycles (0 = start; 1 = end) with different heart rates.

Table 1

Measured aortic blood pressure (BP; units of mmHg and represented as systolic/diastolic) and heart rate (HR; units of beats/minute). All numbers are average values determined by selecting a range of cardiac cycles that correspond to the physiologic interventions (i.e., baseline, increased preload, and increased afterload) and pumping mode (i.e., continuous and pulsed).

		Baseline				Increased Preload				Increased Afterload			
		Continuous		Pulsed		Continuous		Pulsed		Continuous		Pulsed	
		BP	HR	BP	HR	BP	HR	BP	HR	BP	HR	BP	HR
Centrifugal	1	63/38	136	72–35	136	67/37	145	77/34	146	90/44	153	96/40	154
	2	69/35	96	69/27	98	68/25	86	72/19	77	84/41	140	87/34	142
Axial	1	59/43	89	50/40	89	64/38	138	64/38	138	73/46	149	71/45	149
	2	76/42	132	76/41	132	76/28	115	75/28	115	86/44	149	85/43	148

Table 2

Mean aortic flow (i.e., essentially cardiac output) and mean flow provided by the LVAD (units of L/minute). All numbers are average values determined by selecting a range of cardiac cycles that correspond to the physiologic interventions (i.e., baseline, increased preload, and increased afterload) and pumping mode (i.e., continuous and pulsed).

		Baseline				Increased Preload				Increased Afterload			
		Continuous		Pulsed		Continuous		Pulsed		Continuous		Pulsed	
		Aortic	Pump	Aortic	Pump	Aortic	Pump	Aortic	Pump	Aortic	Pump	Aortic	Pump
Centrifugal	1	1.06	3.20	1.86	2.20	0.95	3.15	1.81	2.15	1.85	2.85	2.50	1.80
	2	1.04	2.79	1.66	1.91	1.19	3.05	1.57	2.24	1.76	2.34	2.57	1.24
Axial	1	0.63	2.06	0.61	2.15	1.08	2.63	1.10	2.59	1.02	2.24	0.81	2.27
	2	0.87	3.06	1.01	2.94	1.10	3.53	1.05	3.50	1.65	3.22	1.73	3.14

Table 3

Peak forward compression, decompression wave intensity (units of W/m^2), and forward wave energy (units of J/m^2).

		Baseline			Increased Preload			Increased Afterload		
		C	**CtP**	**CoP**	**C**	**CtP**	**CoP**	**C**	**CtP**	**CoP**
Centrifugal	Peak forward compression wave intensity	11.3±0.1	12.3±0.1 *	12.0±0.1 *	13.9±0.2	15.4±0.5	14.5±0.5	20.6±0.3	20.3±0.3	19.6±0.3
	Peak forward decompression wave intensity	4.6±0.2	5.5±0.3	5.4±0.3	7.0±0.1	7.3±0.1	7.2±0.1	8.4±0.2	9.9±0.3 *	9.9±0.3 *
	Forward wave energy	0.50±0.01	0.55±0.01 *	0.52±0.01	0.56±0.01	0.57±0.01	0.56±0.01	0.71±0.01	0.73±0.01	0.71±0.01
Axial	Peak forward compression wave intensity	3.4±0.1	3.6±0.1	3.7±0.1 *	3.0±0.0	2.9±0.0	2.9±0.1	6.4±0.1	6.8±0.1	6.6±0.1
	Peak forward decompression wave intensity	5.8±0.1	5.8±0.1	6.0±0.1	5.0±0.1	5.1±0.1	5.1±0.1	9.2±0.1	9.6±0.1 *	9.6±0.1 *
	Forward wave energy	0.57±0.01	0.57±0.01	0.59±0.01	0.49±0.00	0.49±0.00	0.49±0.00	0.75±0.00	0.77±0.00	0.76±0.00

Data are mean values ± standard error of the mean. Statistical results are from one-way ANOVA and Bonferroni comparisons between continuous (C), counter-pulse (CtP), and co-pulse (CoP) within each condition.

*($p < 0.05$) indicates a comparison to continuous and

†($p < 0.05$) indicates a comparison to counter-pulse.